Numerical Subgrid Upscaling for Waterflood Simulations

Todd Arbogast, SPE, and Steven L. Bryant, Center for Subsurface Modeling, Texas Institute for Computational and Applied Mathematics, The University of Texas at Austin

Abstract

We present a subgrid-scale numerical technique for upscaling waterflood simulations. We scale up the usual parameters porosity and relative and absolute permeabilities, and also the location of wells and capillary pressure curves. Some of these are critical nonlinear terms that need to be resolved on the fine scale, or serious errors will result. Upscaling is achieved by explicitly decomposing the differential system into a coarse-grid-scale operator coupled to a subgrid-scale operator. The subgrid-scale operator is approximated as an operator localized in space to a coarse-grid element. An influence function (numerical Greens function) technique allows us to solve these subgrid-scale problems independently of the coarse-grid approximation. The coarse-grid problem is modified to take into account the subgrid-scale solution and solved as a large linear system of equations. Finally, the coarse scale solution is corrected on the subgrid-scale, providing a fine-grid scale representation of the solution. In this approach, no explicit macroscopic coefficients nor pseudo-functions result. The method is easily seen to be optimally convergent in the case of a single linear parabolic equation. The method is several times faster than solving the fine-scale problem directly, generally more robust, and yet achieves good results as it requires no ad hoc assumptions at the coarse scale and retains all the physics of the original multiphase flow equations.

Introduction

There is a large and growing literature on upscaling techniques. We will not attempt a literature review here, but merely mention a few of the main techniques. The first and basic techniques developed involved in an essential way averaging or homogenization of physical parameters such as permeability (see, e.g., [1], [2], [3]). While such upscaling techniques can be very effective for purely linear problems, they are less satisfactory for nonlinear problems. They suffer from the elementary observation that a nonlinear function of an average is not the average of the nonlinear function. For example, over a coarse grid-block, the value of capillary pressure evaluated at the average saturation is not at all the same as the average over the grid-block of the capillary pressure.

More sophisticated techniques have been developed to circumvent the inadequacies of simple averaging (see, e.g., [4], [5], [6], [7]), including the development of renormalization techniques to successively upscale to coarse levels, pseudo-functions, modified finite element basis functions, and explicit subgrid techniques that seek to improve the resolution of the coarse solution after it has been computed. These techniques all attempt in some way to represent fine-scale information on coarse scales in an indirect way, and sometimes require at least some information about the nature of the flow that is expected under field management conditions. Although most upscaling techniques are dynamic in that they respond to the changing state of the reservoir, many do so through anticipation of the possibilities. Often one needs some kind of closure assumption such as the imposition of local boundary conditions, the expected primary flow direction, or expected limits on certain parameters such as flow rates.

To handle the dynamic and sometimes unanticipated nature of reservoir conditions, we present in this paper an implicit subgrid technique that allows us to upscale the pressure equation, and discuss its implementation in a sequential two-phase water-flood research simulator. We maintain a fully implicit (as opposed to an explicit) coupling between the coarse and fine or subgrid scales, and we obtain a fine-scale representation of the reservoir state. As a consequence, we make use of the capillary pressure and relative permeability curves directly and accurately on the fine-scale on which

they are defined. No pseudo-functions are needed, nor do any arise in our technique. Our technique allows us to upscale heterogeneous absolute permeability and porosity, the non-linear functions relative permeability and capillary pressure, and even the fine scale position of wells.

The idea is to consider the simulation as defined on a fine grid, and to de-refine this grid to form a reasonable coarse grid over which we can compute the solution. We break the solution into two parts, the coarse-scale representation of the solution plus the subgrid part. The subgrid part is defined inside the coarse grid blocks. In order to be able to compute it efficiently, it must involve only the coarse solution itself and local information. Because of this computational restriction and the need to maintain accuracy, we compute the coarse-scale Darcy velocity using a second order accurate method. Thus, even though the coarse part of the velocity has accuracy based on the coarse-scale resolution H (the diameter of a coarse grid block), the expected accuracy is actually proportional to H^2. Thus the coarse-scale velocity is accurate from the point of view of the subgrid-scale, for which we use a more standard first order accurate method such as cell-centered finite differences. The use of a low order method for the solution on the subgrid scale is natural, since, e.g., heterogeneities in the permeability are likely to produce solutions with large spatial gradients. It is well-known that higher order methods do not in general improve such solutions much, and certainly not enough to justify the added cost.

Because we insist upon an implicit coupling between the coarse and subgrid scales, there will be a mixture of these two parts of our solution in the equations. Some kind of static condensation or Schur complement technique is needed to eliminate the subgrid unknowns from the equations. We do this using a technique involving numerical Greens functions (also called influence functions). This technique allows us to treat the subgrid and coarse scales in completely separate parts of the computer code. It is also relatively memory efficient.

To maintain local mass conservation, our procedure is based on mixed finite element methods [8], [9]. It is known that the lowest order Raviart-Thomas method [10], RT0, when combined with numerical quadrature to evaluate some of the integrals that arise, is the same as cell-centered finite differences. A similar method that gives higher order velocities uses the finite element spaces defined in 2-D by Brezzi, Douglas, and Marini [11], BDM1, and generalized in 3-D by Brezzi, Douglas, Duràn and Fortin [12], BDDF1.

The Numerical Subgrid Upscaling Method for the Pressure Equation

In this section we present in some detail the technique described briefly in the Introduction. Because of the need for a higher order accurate coarse solution, we must present the technique in a finite element context rather than a cell-centered finite difference context.

The pressure equation. In order to simplify the presentation, we illustrate our ideas on the differential equations

$$a\,P + \nabla \cdot \mathbf{u} = b \ , \tag{1}$$

$$\mathbf{u} = -d(\nabla P - c) \ , \tag{2}$$

where a, b, c and d are constants. The pressure equation is an example of such a system, as we will see later.

The finite element basis functions. In a mixed finite element method, finite element basis functions are used to approximate both the pressure P and the Darcy velocity $\mathbf{u}$. The Darcy velocity is *not* defined from the pressure as a simple finite difference involving nearby pressures; in fact, it is defined from *all* the pressures in the reservoir, although the nearby ones are the most important. That is, $\mathbf{u}$ is *not* defined from P through a *finite* stencil or molecule, and so the method does not reduce to finite differences. (However, as noted in [13] and [14] for RT0, we can approximate $\mathbf{u}$ as a finite stencil of the pressures, and recover the usual 7 point stencil, or even a 19-point stencil if the permeability is a full tensor [15].)

Pressure basis functions. In both the RT0 and BDDF1 (or BDM1) spaces, the pressure is approximated by a piecewise discontinuous constant function. That is, the pressure is approximated on each grid block by a constant value, just like it is in cell-centered finite differences. Such functions are linear combinations of simpler basis functions. Let us number the coarse grid blocks $1, 2, ..., N$. For the ith coarse grid block, there is a pressure basis function, call it $\bar{w}_i$, which takes the value 1 on the block and 0 everywhere else. Within each coarse grid block are similar subgrid-scale basis functions. Suppose that there are M_i fine grid blocks in the ith coarse grid block. For each $k = 1, 2, ..., M_i$, we let $\hat{w}_k^i$ be 1 on the kth subgrid block and 0 everywhere else.

In a finite element method, we approximate the pressure in the finite element space; thus, defining both a coarse and subgrid pressure, we have that for any point $\mathbf{x}$ in the reservoir,

$$\bar{P}(\mathbf{x}) = \sum_{i=1}^{N} \alpha_i \bar{w}_i(\mathbf{x}) \ , \tag{3}$$

$$\hat{P}(\mathbf{x}) = \sum_{i=1}^{N} \sum_{k=1}^{M_i} \beta_k^i \hat{w}_k^i(\mathbf{x}) \ , \tag{4}$$

$$P(\mathbf{x}) = \bar{P}(\mathbf{x}) + \hat{P}(\mathbf{x}) \ , \tag{5}$$

where the coefficients α_i and β_k^i are to be determined. Even though our intent is to upscale, we have in fact a pressure value for each fine grid block, as illustrated in Fig. 1.

Velocity basis functions. The velocity is a vector, so the velocity basis functions are also vector functions. We describe the basis functions as if the grid block was simply the unit cube $0 \le x \le 1$, $0 \le y \le 1$, and $0 \le z \le 1$. There are 6

basis functions common to RT0 and BDDF1, which have a nonzero divergence. These are given by

$$\tilde{\mathbf{v}}_1 = (1 - x)\mathbf{e}_1 \ ,$$
$$\tilde{\mathbf{v}}_2 = x\mathbf{e}_1 \ ,$$
$$\tilde{\mathbf{v}}_3 = (1 - y)\mathbf{e}_2 \ ,$$
$$\tilde{\mathbf{v}}_4 = y\mathbf{e}_2 \ ,$$
$$\tilde{\mathbf{v}}_5 = (1 - z)\mathbf{e}_3 \ ,$$
$$\tilde{\mathbf{v}}_6 = z\mathbf{e}_3 \ .$$

There is one function for each face of the grid block, and each represents a unit flow either into or out of the block across that face, and no flow across the other faces. For example $\tilde{\mathbf{v}}_1$ gives a unit flow into the block across the face $x = 0$, while $\tilde{\mathbf{v}}_2$ gives a unit flow out of the block across $x = 1$.

The BDDF1 spaces have the 12 additional basis functions

$$\tilde{\mathbf{v}}_7 = (1 - x)(2y - 1)\mathbf{e}_1 + (y^2 - y)\mathbf{e}_2 \ ,$$
$$\tilde{\mathbf{v}}_8 = x(2y - 1)\mathbf{e}_1 + (y - y^2)\mathbf{e}_2 \ ,$$
$$\tilde{\mathbf{v}}_9 = (x^2 - x)\mathbf{e}_1 + (1 - y)(2x - 1)\mathbf{e}_2 \ ,$$
$$\tilde{\mathbf{v}}_{10} = (x - x^2)\mathbf{e}_1 + y(2x - 1)\mathbf{e}_2 \ ,$$
$$\tilde{\mathbf{v}}_{11} = (x^2 - x)\mathbf{e}_1 + (1 - z)(2x - 1)\mathbf{e}_3 \ ,$$
$$\tilde{\mathbf{v}}_{12} = (x - x^2)\mathbf{e}_1 + z(2x - 1)\mathbf{e}_3 \ ,$$
$$\tilde{\mathbf{v}}_{13} = (1 - x)(2z - 1)\mathbf{e}_1 + (z^2 - z)\mathbf{e}_3 \ ,$$
$$\tilde{\mathbf{v}}_{14} = x(2z - 1)\mathbf{e}_1 + (z - z^2)\mathbf{e}_3 \ ,$$
$$\tilde{\mathbf{v}}_{15} = (1 - y)(2z - 1)\mathbf{e}_2 + (z^2 - z)\mathbf{e}_3 \ ,$$
$$\tilde{\mathbf{v}}_{16} = y(2z - 1)\mathbf{e}_2 + (z - z^2)\mathbf{e}_3 \ ,$$
$$\tilde{\mathbf{v}}_{17} = (y^2 - y)\mathbf{e}_2 + (1 - z)(2y - 1)\mathbf{e}_3 \ ,$$
$$\tilde{\mathbf{v}}_{18} = (y - y^2)\mathbf{e}_2 + z(2y - 1)\mathbf{e}_3 \ .$$

Each has vanishing divergence, so these basis functions represent no net flow. They merely redistribute flow across the face from one side to the other. For example, the $\tilde{\mathbf{v}}_7$ represents a redistribution of flow on the $x = 0$ face, by allowing flow into the block on the $y = 0$ side and taking it back out on the $y = 1$ side. The function $\tilde{\mathbf{v}}_{13}$ is similar, except that flow is redistributed in the z direction.

For an arbitrary rectangular grid block, we translate and scale these functions. It should be noted that $\tilde{\mathbf{v}}_7$ to $\tilde{\mathbf{v}}_{18}$ must be scaled so that the divergence remains zero. For example, $\tilde{\mathbf{v}}_7$ becomes

$$\tilde{\mathbf{v}}_7 = (1 - x/h_x)(2y/h_y - 1)\mathbf{e}_1 + (y^2/h_y - y)/h_x\mathbf{e}_2 \ .$$

For consistency of flow, these basis functions are paired across grid blocks. For example, two blocks that share an x face would have $\tilde{\mathbf{v}}_2$ on the left and $\tilde{\mathbf{v}}_1$ on the right, or $\tilde{\mathbf{v}}_8$ on the left and $\tilde{\mathbf{v}}_7$ on the right. Thus there are 3 basis functions per grid block face for BDDF1, and 1 for RT0. (In 2-D, the RT0 and BDM1 spaces are similar, except that only $\tilde{\mathbf{v}}_1$ to $\tilde{\mathbf{v}}_4$ and $\tilde{\mathbf{v}}_7$ to $\tilde{\mathbf{v}}_{10}$ arise.)

In our subgrid approach, we need 3 BDDF1 basis functions defined for each coarse grid block face. Call these basis functions $\bar{\mathbf{v}}_j$, $j = 1, 2, ..., N'$. Within coarse grid block i, we need RT0 basis functions defined for each fine grid block face, which we denote by $\hat{\mathbf{v}}_\ell^i$, $\ell = 1, 2, ..., M_i'$. Finally, defining both a coarse and subgrid velocity, we have that

$$\bar{\mathbf{u}}(\mathbf{x}) = \sum_{j=1}^{N'} \gamma_j \bar{\mathbf{v}}_j(\mathbf{x}) \ , \tag{6}$$

$$\hat{\mathbf{u}}(\mathbf{x}) = \sum_{i=1}^{N} \sum_{\ell=1}^{M_i'} \delta_\ell^i \hat{\mathbf{v}}_\ell^i(\mathbf{x}) \ , \tag{7}$$

$$\mathbf{u}(\mathbf{x}) = \bar{\mathbf{u}}(\mathbf{x}) + \hat{\mathbf{u}}(\mathbf{x}) \ , \tag{8}$$

where the coefficients γ_j and δ_ℓ^i are to be determined.

As illustrated in Fig. 1, the velocity has 3 fluxes (2 in 2-D) on each coarse grid block face representing flow between the grid blocks that varies linearly over the face, and a single constant flux across fine grid block faces that lie within the coarse grid blocks. Thus we have good resolution. It is the special placement of these fluxes, i.e., these finite element nodal values, that allows us to upscale.

The direct finite element formulation. Multiply each equation (1)–(2) by a finite element basis function, which is called a test function, and integrate. Let w be any of the $\bar{w}_i$ or $\hat{w}_k^i$, and $\mathbf{v}$ be any of the $\bar{\mathbf{v}}_j$ or $\hat{\mathbf{v}}_\ell^i$. This results in the equations

$$\int a\, P\, w\, dV + \int \nabla \cdot \mathbf{u}\, w\, dV = \int b\, w\, dV \ , \tag{9}$$

$$\int d^{-1}\mathbf{u} \cdot \mathbf{v}\, dV = -\int \nabla P \cdot \mathbf{v}\, dV + \int c \cdot \mathbf{v}\, dV$$
$$= \int P\, \nabla \cdot \mathbf{v}\, dV + \int c \cdot \mathbf{v}\, dV \ , \tag{10}$$

where we have made use of the divergence theorem to replace $-\int \nabla P \cdot \mathbf{v}\, dV$ by $\int P\, \nabla \cdot \mathbf{v}\, dV$, since there is no flow on the external boundary of the reservoir (if other boundary conditions are used, certain boundary terms appear at this stage, but otherwise no particular complications arise later).

Combining (9)–(10) with (3)–(5) and (6)–(8) results in a fully implicit system of linear equations, a square matrix problem of size $N + \sum_i M_i + N' + \sum_i M_i'$, for the unknowns α_i, β_k^i, γ_j, and δ_ℓ^i. This system is too large to solve as formulated, so we will not discuss its implementation. It has nearly as many unknowns as the fine scale solution itself: the same number of pressures, and as many velocity fluxes within the coarse blocks. On the faces of the coarse blocks, we have fewer velocity fluxes than one would have in a fine scale solution, but these fluxes are higher-order accurate and so give a good approximation of the velocity.

The system is actually underdetermined, since the pressure basis functions sum to 1, i.e., $\sum_{k=1}^{M_i} \hat{w}_k^i = \bar{w}_i$. That is, the decomposition of P into $\bar{P}$ and $\hat{P}$ is not unique. The

removal of this ambiguity depends on the nature of a. For each coarse block i, if $a = 0$ on the block, we cannot solve our subgrid problems below as they are written. Instead, we remove, say, the test function $w = \hat{w}_1^i$ and replace that equation by the requirement that

$$\int \hat{P} \, \bar{w}_i \, dV = 0 \ . \tag{11}$$

If, however, $a \neq 0$ on the block, then we can solve our subgrid problems below as written (i.e., we do not replace the $w = \hat{w}_1^i$ equation as above), and we require either (11) or instead

$$\int a \hat{P} \, \bar{w}_i \, dV = 0 \ , \tag{12}$$

as we will make clear later. In both cases, however, we can solve our equations, and the decomposition $P = \bar{P} + \hat{P}$ is unique.

Our goal now is to exploit our choice of basis functions so that the system can be solved in smaller steps, with the last step being the solution of a substantially reduced matrix problem of size $(N+N') \times (N+N')$ involving only the coarse scale unknowns α_i and γ_j. That is, we upscale to the coarse level. We emphasize that we are not changing the method below, but merely describing how to obtain the solution. Our solution technique requires 3 steps; no iteration is performed.

Numerical Greens Functions. The key is to use numerical Greens functions, also known as influence functions. The idea can be illustrated in a trivial example. Suppose we want to solve $ax + by + cz = d$ for x in terms of y and z, which are not known. The solution is obviously $x = (d - by - cz)/a$. We can arrive at this same result by solving three problems that involve neither y nor z as follows. First set $y = z = 0$ and solve $ax_0 = d$. Next set the nonhomogeneous terms to 0 (i.e., d=0), set $y = 1$ and $z = 0$, and solve $ax_1 = -b$. Finally, set $d = 0$, $y = 0$, and $z = 1$ and solve $ax_2 = -c$. Then the solution is the combination of these simple solutions: $x = x_0 + x_1 y + x_2 z$.

Note that x_1 gives the influence of y on x ($x_1 = \partial x/\partial y$) and x_2 gives the influence of z on x ($x_2 = \partial x/\partial z$). Alternatively, one can view x_1 as the response of the system to a unit stimulus in y, that is, a Greens function, and similarly for x_2 and z.

This technique works even when x is a vector, a is a matrix, and b, c, and d are vectors.

In our case, we apply the idea to each coarse grid block. On the ith block, x refers to the subgrid unknowns β_k^i and δ_ℓ^i, and y and z refer to the coarse block unknowns α_i and all γ_j for which $\bar{\mathbf{v}}_j$ lives (i.e., is not zero) on the ith block. We have arranged that there are very few such coarse block unknowns.

The upscaled finite element formulation. We begin by solving the subset of equations (9)–(10) for which the test functions live on the subgrid scale. These subgrid equations

are coupled to the coarse-scale. On coarse block i, the subgrid is affected only by the coarse coefficients α_i and the 18 γ_j for which $\bar{\mathbf{v}}_j$ lives on the block. Because of (11)–(12), we have arranged the computation so that α_i, i.e., the coarse pressure $\bar{P}$, does not affect the subgrid scale. Thus only 18 parameters affect the subgrid scale, and we can determine the influence of each through the numerical Greens function approach.

Step 1: The subgrid problems. For coarse block i, consider (9)–(10) with test functions $w = \hat{w}_{k'}^i$ and $\mathbf{v} = \hat{\mathbf{v}}_{\ell'}^i$. In the numerical Greens function approach, we first solve assuming the coarse scale information is set to zero. Solve for

$$\hat{P}_0^i = \sum_{k=1}^{M_i} \beta_{0,k}^i \hat{w}_k^i \ , \tag{13}$$

$$\hat{\mathbf{u}}_0^i = \sum_{\ell=1}^{M_i'} \delta_{0,\ell}^i \hat{\mathbf{v}}_\ell^i \ , \tag{14}$$

the equations represented by

$$\int a \hat{P}_0^i \hat{w}_{k'}^i \, dV + \int \nabla \cdot \hat{\mathbf{u}}_0^i \, \hat{w}_{k'}^i \, dV = \int b \, \hat{w}_{k'}^i \, dV \ , \tag{15}$$

$$\int d^{-1} \hat{\mathbf{u}}_0^i \cdot \hat{\mathbf{v}}_{\ell'}^i \, dV$$
$$= \int \hat{P}_0^i \, \nabla \cdot \hat{\mathbf{v}}_{\ell'}^i \, dV + \int c \cdot \hat{\mathbf{v}}_{\ell'}^i \, dV \ . \tag{16}$$

In matrix form, these equations are

$$\sum_{k=1}^{M_i} \beta_{0,k}^i \int a \, \hat{w}_k^i \, \hat{w}_{k'}^i \, dV + \sum_{\ell=1}^{M_i'} \delta_{0,\ell}^i \int \nabla \cdot \hat{\mathbf{v}}_\ell^i \, \hat{w}_{k'}^i \, dV$$
$$= \int b \, \hat{w}_{k'}^i \, dV \ , \tag{17}$$

$$\sum_{\ell=1}^{M_i'} \delta_{0,\ell}^i \int d^{-1} \hat{\mathbf{v}}_\ell^i \cdot \hat{\mathbf{v}}_{\ell'}^i \, dV$$
$$= \sum_{k=1}^{M_i} \beta_{0,k}^i \int \hat{w}_k^i \, \nabla \cdot \hat{\mathbf{v}}_{\ell'}^i \, dV + \int c \cdot \hat{\mathbf{v}}_{\ell'}^i \, dV \ . \tag{18}$$

We then solve for the influence of each $\bar{\mathbf{v}}_j$ living on the ith block. There are 18 such j. We solve for

$$\hat{P}_j^i = \sum_{k=1}^{M_i} \beta_{j,k}^i \hat{w}_k^i \ , \tag{19}$$

$$\hat{\mathbf{u}}_j^i = \sum_{\ell=1}^{M_i'} \delta_{j,\ell}^i \hat{\mathbf{v}}_\ell^i \ , \tag{20}$$

the equations represented by

$$\int a \hat{P}_j^i \hat{w}_{k'}^i \, dV + \int \nabla \cdot (\bar{\mathbf{v}}_j + \hat{\mathbf{u}}_j^i) \, \hat{w}_{k'}^i \, dV = 0 \ , \tag{21}$$

$$\int d^{-1} (\bar{\mathbf{v}}_j + \hat{\mathbf{u}}_j^i) \cdot \hat{\mathbf{v}}_{\ell'}^i \, dV = \int \hat{P}_j^i \, \nabla \cdot \hat{\mathbf{v}}_{\ell'}^i \, dV \ . \tag{22}$$

In matrix form, we have

$$
\sum_{k=1}^{M_i} \beta_{j,k}^i \int a\,\hat{w}_k^i\,\hat{w}_{k'}^i\,dV + \sum_{\ell=1}^{M_i'} \delta_{j,\ell}^i \int \nabla\cdot\hat{\mathbf{v}}_\ell^i\,\hat{w}_{k'}^i\,dV
$$
$$
= -\int \nabla\cdot\bar{\mathbf{v}}_j\,\hat{w}_{k'}^i\,dV \ , \tag{23}
$$

$$
\sum_{\ell=1}^{M_i'} \delta_{j,\ell}^i \int d^{-1}\hat{\mathbf{v}}_\ell^i\cdot\hat{\mathbf{v}}_{\ell'}^i\,dV
$$
$$
= \sum_{k=1}^{M_i} \beta_{j,k}^i \int \hat{w}_k^i\,\nabla\cdot\hat{\mathbf{v}}_{\ell'}^i\,dV - \int d^{-1}\bar{\mathbf{v}}_j\cdot\hat{\mathbf{v}}_{\ell'}^i\,dV \ . \tag{24}
$$

We must insist that the normalization (11) applies to $\hat{P}_0^i$, and that (11) or (12) apply to each $\hat{P}_j^i$, depending on whether $a=0$ or not. This normalization is done either before trying to solve the equations if $a=0$ on the block, or otherwise after obtaining the solution.

We use a direct solver in this step, since there are multiple right-hand sides (19 in all), and these problems are generally small (at most the subgrid is perhaps $10\times10\times10$). These problems also parallelize trivially.

Once this step is complete, then we have the formal representation of the subgrid solution on coarse block i as

$$
\hat{P} = \hat{P}_0^i + \sum_j \gamma_j \hat{P}_j^i = \sum_{k=1}^{M_i}\left(\beta_{0,k}^i + \sum_j \gamma_j \beta_{j,k}^i\right)\hat{w}_k^i \ , \tag{25}
$$

$$
\hat{\mathbf{u}} = \hat{\mathbf{u}}_0^i + \sum_j \gamma_j \hat{\mathbf{u}}_j^i = \sum_{\ell=1}^{M_i'}\left(\delta_{0,\ell}^i + \sum_j \gamma_j \delta_{j,\ell}^i\right)\hat{\mathbf{v}}_\ell^i \ . \tag{26}
$$

Thus

$$
\beta_k^i = \beta_{0,k}^i + \sum_j \gamma_j \beta_{j,k}^i \ , \tag{27}
$$

$$
\delta_\ell^i = \delta_{0,\ell}^i + \sum_j \gamma_j \delta_{j,\ell}^i \ . \tag{28}
$$

We know every quantity above except the γ_j, so these are not yet computable. However, these formulas can be used in the coarse scale equations to obtain a linear system for the α_i and γ_j only.

Step 2: The upscaled coarse problem. In the second step, we solve the upscaled coarse problem, which is given by (9)–(10) with the test functions which live on the coarse scale $w=\bar{w}_{i'}$ and $\mathbf{v}=\bar{\mathbf{v}}_{j'}$. This system, when combined with (25)–(26), gives a matrix problem for the α_i and γ_j. It is derived in

detail in the Appendix. The system is

$$
\sum_{i=1}^N \alpha_i \int a\,\bar{w}_i\,\bar{w}_{i'}\,dV + \sum_{j=1}^{N'} \gamma_j \int \nabla\cdot\bar{\mathbf{v}}_j\,\bar{w}_{i'}\,dV
$$
$$
= \int (b - a\hat{P}_0)\,\bar{w}_{i'}\,dV \ , \tag{29}
$$

$$
\sum_{j=1}^{N'} \gamma_j \left\{ \int d^{-1}(\bar{\mathbf{v}}_j + \hat{\mathbf{u}}_j)\cdot(\bar{\mathbf{v}}_{j'} + \hat{\mathbf{u}}_{j'})\,dV \right.
$$
$$
\left. + \int a\,\hat{P}_j\,\hat{P}_{j'}\,dV \right\}
$$
$$
= \sum_{i=1}^N \alpha_i \int \bar{w}_i\,\nabla\cdot\bar{\mathbf{v}}_{j'}\,dV + \int (c - d^{-1}\hat{\mathbf{u}}_0)\cdot\bar{\mathbf{v}}_{j'}\,dV \ , \tag{30}
$$

where, of coarse, $\hat{P}_j$ is $\hat{P}_j^i$ and $\hat{\mathbf{u}}_j$ is $\hat{\mathbf{u}}_j^i$ whenever we integrate over the ith coarse grid block.

If the subgrid scale influence functions are set to zero, this is a BDDF1 mixed finite element discretization of the pressure equations representing conservation of mass and Darcy's law. The upscaled equations represent a coarse grid conservation of mass and a coarse grid Darcy law, with the matrix coefficients modified by the subgrid-scale influence functions. Thus to implement, one first develops a code to handle the BDDF1 method on the coarse-grid, and then modifies the integration routines to solve (29)–(30).

Step 3: The fine-scale representation of the solution. Finally, we construct a fine-scale representation of our solution by combining the previous results to obtain

$$
P = \bar{P} + \sum_{i=1}^N \left(\hat{P}_0^i + \sum_j \gamma_j \hat{P}_j^i\right)
$$
$$
= \sum_{i=1}^N \left[\alpha_i\bar{w}_i + \sum_{k=1}^{M_i}\left(\beta_{0,k}^i + \sum_j \gamma_j \beta_{j,k}^i\right)\hat{w}_k^i\right], \tag{31}
$$

$$
\mathbf{u} = \bar{\mathbf{u}} + \sum_{i=1}^N \left(\hat{\mathbf{u}}_0^i + \sum_j \gamma_j \hat{\mathbf{u}}_j^i\right)
$$
$$
= \sum_{j=1}^{N'} \gamma_j\bar{\mathbf{v}}_j + \sum_{i=1}^N \sum_{\ell=1}^{M_i'}\left(\delta_{0,\ell}^i + \sum_j \gamma_j \delta_{j,\ell}^i\right)\hat{\mathbf{v}}_\ell^i \ . \tag{32}
$$

This is precisely the solution to (9)–(10).

In summary, in Step 1, we solve in parallel (17)–(18) and (23)–(24), possibly modified as mentioned in (11) for solvability, for each coarse grid block i for the coefficients of the numerical Greens functions (or influence functions). We then construct $\hat{P}_0^i$, $\hat{\mathbf{u}}_0^i$, $\hat{P}_j^i$, and $\hat{\mathbf{u}}_j^i$ using (13)–(14), and normalize by (11) or (12) if this was not already done for solvability. In Step 2, we solve the upscaled equations (29)–(30) for the coarse coefficients α_i and γ_j. This gives part of our solution $\bar{P}$ and $\bar{\mathbf{u}}$. Finally, in Step 3, we construct a fine-scale representation of our solution from (31)–(32). This is precisely the solution to (9)–(10).

Application to Two-Phase Incompressible, Immiscible Flow

We can easily adapt our upscaling technique to two-phase immiscible flow if the system is written as a pressure equation coupled to a saturation equation. While our technique could be adapted for a fully implicit system, we chose to develop a research simulator that used a sequential approach. Thus both the pressure and saturation equations are individually fully implicit, but they are decoupled in time. We solve for the pressure using the saturation at the previous time, update the velocities, and then advance the saturation.

The formulation of the equations. We use the standard two-phase flow equations; however, they are formulated in a somewhat nonstandard way. This has no bearing on the numerical upscaling technique, but we mention it for completeness.

The global pressure formulation. The formulation of the pressure equation that we use is due to Chavent [16]. When the fluids are incompressible, we can define a "global" pressure P from one of the phase pressures and the saturation S as

$$P = P_o + \int_S^1 \frac{\lambda_w(s)}{\lambda(s)} P_c'(s) \, ds \; , \qquad (33)$$

where $\lambda_w(S) = k_{r,w}(S)/\mu_w$ and $\lambda_o(S) = k_{r,o}(S)/\mu_o$ are the relative mobilities, and $\lambda(S) = \lambda_w(S) + \lambda_o(S)$. Then

$$\lambda \nabla P = \lambda_w \nabla P_w + \lambda_o \nabla P_o \; ,$$

and, with $\mathbf{u} = \mathbf{u}_w + \mathbf{u}_o$ being the total velocity, we have the pressure equation

$$\frac{\partial \phi}{\partial t} + \nabla \cdot \mathbf{u} = q(P) \; , \qquad (34)$$

$$\mathbf{u} = -K\lambda(S)\big(\nabla P - \rho(S)\mathbf{e}_3\big) \; , \qquad (35)$$

where $q(P) = q_w + q_o$ represents the total flow of the wells and the density is

$$\rho(S) = \frac{\lambda_w(S)}{\lambda(S)}\rho_w + \frac{\lambda_o(S)}{\lambda(S)}\rho_o \; . \qquad (36)$$

With S being fixed in the equation to its value at the previous time step, this equation is the same as (1)–(2) if the time derivative is replaced with a backward finite difference and $q(P)$ is an affine function. Generally one assumes the rock compressibility is constant, so $\phi = \phi(P)$ is itself affine. If $q(P)$ is not affine, we linearize it in a Newton-Raphson procedure to obtain an equation of the form (1)–(2).

The Kirchhoff saturation formulation. The saturation equation is formulated so as to use a standard fractional flow, but with the diffusive terms modified with a Kirchhoff transformation [17]. That is, we have

$$\frac{\partial \phi S}{\partial t} + \nabla \cdot \mathbf{u}_w = q_w(S) \; , \qquad (37)$$

$$\mathbf{u}_w = -K\nabla Q(S) + c(\mathbf{u}, S) \; , \qquad (38)$$

where the "complementary" potential Q and c are given by

$$Q(S) = -\int_0^S \frac{\lambda_w(s)\lambda_o(s)}{\lambda(s)} P_c'(s) \, ds \; , \qquad (39)$$

$$c(\mathbf{u}, S) = \frac{\lambda_w(S)}{\lambda(S)}\left[\mathbf{u} - K\lambda_o(S)(\rho_o - \rho_w)g\mathbf{e}_3\right]. \qquad (40)$$

In the sequential approach, we have already solved for $\mathbf{u}$, and we use its fine-scale representation here. After replacing the time derivative with a backward finite difference, and after a Newton linearization, this equation is also of the form (1)–(2).

We can adapt our upscaling idea to the saturation equation, and did so in [18] with a good deal of success. However, because the saturation equation is diagonally dominant, we found that the time savings were marginal when using our particular upscaling technique for the saturation part of the solution. Moreover, in certain difficult problems [19], we found that the use of a higher order method prevented us from satisfying the maximum principle that requires the saturation to lie between its residual and one minus the residual of the other fluid. It is well known that such monotone methods must necessarily be of the first order (if the method itself is linear). Thus, we chose to solve the saturation equation on the fine scale. For simplicity, we used one-point upstream weighting.

Bottom-hole pressure wells. All terms associated with constant rate injection wells have been treated in our description of the upscaling technique, since q is known and fixed. Bottom-hole pressure wells, as modeled by Peaceman [20], present no difficulties either for the upscaling technique or for the global pressure formulation. We have along the well at depth level k,

$$q_{w,k} = -\kappa_{w,k}\big(P_{w,k} - P_{\text{well},k}\big) \; ,$$
$$q_{o,k} = -\kappa_{o,k}\big(P_{o,k} - P_{\text{well},k}\big) \; ,$$
$$P_{\text{well},k} = P_{BHP} + \rho_{\text{well}}g(z_k - z_{BHP}) \; ,$$
$$\rho_{\text{well}} = \frac{\sum_k (q_{w,k}\rho_w + q_{o,k}\rho_o)}{\sum_k (q_{w,k} + q_{o,k})} \; , \qquad (41)$$

where the κ_w and κ_o are given by Peaceman. Thus, using (33),

$$q_k = q_{w,k} + q_{o,k}$$
$$= -(\kappa_{w,k} + \kappa_{o,k})\big(P_k - P_{BHP} - \rho_{\text{well}}g(z_k - z_{BHP})\big)$$
$$\quad - \kappa_{w,k}F_w(S_k) - \kappa_{o,k}F_o(S_k) \; , \qquad (42)$$

where

$$P_w = P + F_w(S) \; ,$$
$$P_o = P + F_o(S) \; ,$$
$$F_o(S) = -\int_S^1 \frac{\lambda_w(s)}{\lambda(s)} P_c'(s) \, ds \; ,$$
$$F_w(S) = F_o(S) - P_c(S) \; .$$

We found it convenient to use the numerical Greens function approach to solve the bottom-hole pressure wells. We let ρ_{well} be our influence parameter and solve for the pressure with ρ_{well} set to 0, and then solve for the pressure again with the nonhomogeneous terms set to 0 and ρ_{well} set to 1. Inspection of (42) shows that both of these equations are linear in P, so they simply result in a modification of a and b in (1)–(2). Finally a nonlinear iteration on (41) determines ρ_{well} and completes the solution.

We have one additional pressure solve for each additional bottom-hole pressure well, so this technique is feasible only for a small number of wells. This implementation of the wells would not be practical in a full field simulation. In the general case, we would need to include the well terms as linearized for a Newton-Raphson procedure. Again, only a and b need to be modified.

Due to the evolution of the simulator, we found it convenient for the saturation equation to incorporate bottom-hole pressure wells in a somewhat unusual way. We took the total injection rate as determined from the pressure equation and divided it into the phases according to their relative mobility.

General Numerical Performance

Before presenting our reservoir simulation examples, we mention a few general features of the upscaling method, and an important modification.

Convergence rate for smooth solutions. We tested the convergence rate of the method in [18] by solving the pressure equation (1)–(2) in cases for which the solution is smooth and known. When the number of subgrid blocks per coarse block is held fixed, the errors in the velocities display second order convergence. This is to be expected for the BDDF1 method, however the RT0 method is only linearly convergent. Thus, the use of higher order coarse elements is indeed sufficient to maintain accuracy, and in fact this higher order is reflected in the subgrid computation.

Savings in computation time. The speed of the upscaling method is difficult to quantify, as it depends on so many factors. In our test cases, we used simply Jacobi preconditioned conjugate gradients. It is well known that such a solver is very easy to implement, but also that it does not perform particularly well. However, we have consistently observed a reduction in the solution times of about a factor of 2 to 10 for our upscaling method compared to solving the fine-scale pressure equation with RT0 (which is essentially standard cell-centered finite differences). Since our method is second order accurate compared to first order for RT0, this is quite a savings in time. The savings in solution time compared to solving the second order accurate fine-scale BDDF1 is much more than a factor of 100 in most cases.

A more nearly optimal solver should close the timing gap somewhat, so these reduction factors should not be taken too literally. What is clear is that it is easier to precondition a smaller, coarser system than a larger, finer one. This is due partly to the reduced size, but also more importantly to the reduction in condition number that an averaged or upscaled problem exhibits. The performance of Jacobi preconditioned conjugate gradients is very sensitive to the condition number, and thus we see good speedup for the upscaled system. Even a more efficient solution strategy will benefit from the improved condition number of the upscaled problem compared to the fine-scale problem. We note in passing that if one wanted to solve the fine-scale problem, one could also use our upscaling technique as a type of preconditioner. In that case, perhaps one would be content with RT0 on the coarse scale.

One additional remark about the computational speed should be made. The upscaling method improves data locality, so there is the potential to reuse more data within high-speed memory caches than one might find in a fine-scale solution technique.

Average permeability for nonsmooth solutions. When solutions are not so smooth, it is possible that the coarse flow is not quite of the proper magnitude. This is due to using the fine-scale permeability in the upscaled equation (30), coefficient d. To remedy this, we can use an averaged permeability $\bar{d}$ in place of d on the left-hand side of the equality. That is, replace $\int d^{-1}(\bar{\mathbf{v}}_j + \hat{\mathbf{u}}_j) \cdot (\bar{\mathbf{v}}_{j'} + \hat{\mathbf{u}}_{j'})\, dV$ by $\int (\bar{d})^{-1}(\bar{\mathbf{v}}_j + \hat{\mathbf{u}}_j) \cdot (\bar{\mathbf{v}}_{j'} + \hat{\mathbf{u}}_{j'})\, dV$, but leave d alone in every other term, especially in the subgrid equations. As we will see in our two reservoir examples, this can bring about an improvement in the overall performance of the upscaling method.

A 3-D Numerical Example

In this section we present numerical results that demonstrate the application of the method described above to some simple test cases. We will compare various upscaled computations against a fine scale computation which we treat as the true solution. We consider a rectangular domain 500m × 250m × 40m with a water injector and a single producer, discretized into 1600 fine scale cells ($20 \times 10 \times 8$). We upscale on a $4 \times 2 \times 2$ coarse grid, corresponding to a 100-fold reduction in the number of cells. The porosity is assumed constant at 0.25 and the permeability field is a realization of a spatially correlated distribution derived from observations on an outcrop. A constant-rate injector fully penetrates the reservoir at ($x = 100$, $y = 75$), while a constant-bottomhole-pressure producer at $x = 400$, $y = 200$ is completed only in the upper 30m of the reservoir. Fig. 2 shows the saturation distribution in a vertical plane containing the injector and a horizontal plane at the bottom of the producer after 0.22 pore volumes of water have been injected. The influence of zones of low permeability is evident in the "islands" of high and low saturation. The upscaled solution (using the fine-scale permeabilities directly for coefficient d in (30)) captures many of these small scale features, as illustrated in Fig. 3. Fig. 4 compares the computed water-oil ratio as a function of pore volumes injected for several schemes for averaging the fine-scale permeabilities to obtain $\bar{d}$. The arithmetic average

is denoted by $ua1$; taking the harmonic average in the flow direction and the arithmetic average in the direction perpendicular to flow is denoted $ua2$; the root mean square average, $ua3$; and the one-third power average, $ua4$. The latter does the best job of capturing the behavior, though it predicts slightly earlier water breakthrough.

An SPE Comparative Solution Example

Our second numerical example is based on the 2-D model described in the 2001 SPE comparative solution project for upscaling. The differences are relatively minor, and consist mainly in not being able to set the bottom-hole pressure properly and setting gravity to zero. The latter was done to avoid complications with the saturation solver, and not due to the pressure equation. Thus our results, though not strictly comparable, do show the potential of numerical subgrid upscaling of the pressure equation.

Fig. 5 shows the fine scale solution after 1000 days of injection. The upscaling approach u captures several of the water channels on the left side of the domain and several of the bypassed regions on the right side, Fig. 6. Using the root mean square averaging scheme in the upscaling smears the saturation profiles, Fig. 7. The horizontal component of the total velocity at 1000 days shows good qualitative agreement between the three computations as shown in Figs. 8, 9, and 10. The straight upscaling approach yields a slightly wider range of velocities than the true solution, while the approach using average permeability yields a somewhat narrower range.

Conclusions

We presented a subgrid upscaling approach that decomposes the governing differential equations into a coarse-grid-scale operator that is coupled to a subgrid-scale operator. The subgrid-scale problems can be solved independently of the coarse-grid approximation thanks to a numerical Greens function technique. The global problem is solved only at the coarse scale, and this solution is corrected at the subgrid scale to obtain the fine-scale representation of the problem. In this way no explicit macroscopic coefficients (e.g., effective permeabilities or pseudo-functions) arise, and thus no assumptions about the physics or the expected flow behavior are required.

We illustrated the implementation of this technique for the flow of two immiscible, incompressible phases. For simplicity the implementation is sequential, solving the flow equation fully implicitly with saturation-dependent quantities evaluated at the previous time step, then solving the saturation equation fully implicitly and on the fine scale. We observed a reduction in pressure solution times by a factor of 2 to 10, though we note that we obtain second order accuracy while the fine-scale solution used for timing comparison is only first-order accurate. Good agreement between the upscaled and fine-scale solutions is observed for test cases in which the the coarse grid contains two orders of magnitude fewer grid blocks. Using an appropriate average of the fine

scale permeabilities may improve the fidelity of the upscaled solution under some conditions.

Nomenclature

$BDDF1$ = first order Brezzi-Douglas-Duràn-Fortin mixed finite element function space

$BDM1$ = first order Brezzi-Douglas-Marini mixed finite element function space

dV = differential of volume

$\mathbf{e}_1$ = unit vector in the x-direction

$\mathbf{e}_2$ = unit vector in the y-direction

$\mathbf{e}_3$ = unit vector in the z-direction

H = coarse-grid block diameter

h = fine-grid block diameter

h_x = grid block length in the x direction

h_y = grid block length in the y direction

h_z = grid block length in the z direction

K = absolute permeability

k_r = relative permeability

M_i = number of fine grid blocks in coarse grid block i

M_i' = number of fine grid block faces internal to coarse grid block i

N = number of coarse grid blocks

N' = 3 times the number of coarse grid block faces

P = pressure

P_c = capillary pressure

Q = Kirchhoff "complementary" potential

q = external well sources and sinks

$RT0$ = lowest order Raviart-Thomas mixed finite element function space

S = water (or gas) saturation

$\mathbf{u}$ = Darcy velocity

$\mathbf{v}$ = velocity test function

$\tilde{\mathbf{v}}$ = velocity test function on the unit cube

w = pressure test function

$\mathbf{x}$ = spatial point

(x, y, z) = spatial point

α = finite element coefficients of coarse pressure

β = finite element coefficients of subgrid pressure

γ = finite element coefficients of coarse velocity

δ = finite element coefficients of subgrid velocity

λ = relative mobility

μ = viscosity

ρ = density

ϕ = porosity

Subscripts and superscripts

i = coarse grid block

j = coarse grid block face

k = subgrid block (or the depth index)

ℓ = subgrid block face

o = oil

w = water (or gas)

Accents

$\bar{}$ = coarse-scale function

$\hat{}$ = subgrid scale function

References

1. Kasap, E., and Lake, L.W.: "An analytical method to calculate the effective permeability tensor of a grid block and its application in an outcrop study," *Proceedings of the 10th SPE Symposium on Reservoir Simulation* held in Houston, Texas (February 6–8, 1989), 355–366.
2. Durlofsky, L.J.: "Numerical calculation of equivalent grid block permeability tensors for heterogeneous porous media," *Water Resources Research* **27** (1991), 699–708.
3. Amaziane, B., Bourgeat, A., and Koebbe, J.: "Numerical simulation and homogenization of two-phase flow in heterogeneous porous media," *Transport in Porous Media* **9** (1991), 519–547.
4. Christie, M.A., Mansfield, M., King, P.R., Barker, J.W., and Culverwell, I.D.: "A renormalization-based upscaling technique for WAG floods in heterogeneous reservoirs," SPE 29127, *Thirteenth Symp. on Reservoir Sim.* (Feb. 1995), 353–361.
5. King, M.J., King, P.R., McGill, C.A., and Williams, J.K.: "Effective properties for flow calculations," *Transport in Porous Media* **20** (1995), 169–196.
6. Espedal, M.S., and Saevareid, O.: "Upscaling of permeability based on wavelet representation, *4th European Conf. on the Math. of Oil Recovery* held in Norway (1994).
7. Hou, T.Y., and Wu, X.H.: "A multiscale finite element method for elliptic problems in composite materials and porous media," *J. Comput. Phys.* **134** (1997), 169–189.
8. Brezzi, F., and Fortin, M.: Mixed and hybrid finite element methods, Springer-Verlag, New York (1991).
9. Durlofsky, L.J.: "Accuracy of mixed and control volume finite element approximations to Darcy velocity and related quantities," *Water Resources Research* (1994) **30**, 965–973.
10. Raviart, R.A., and Thomas, J.M.: "A mixed finite element method for 2nd order elliptic problems," in *Mathematical Aspects of the Finite Element Method*, Lecture Notes in Math. 606, Springer-Verlag, New York (1977), 292–315.
11. Brezzi, F., Douglas, J., Jr., and Marini, L.D.: "Two families of mixed elements for second order elliptic problems," *Numer. Math.* (1985) **88**, 217–235.
12. Brezzi, F., Douglas, J., Jr., Duràn, R., and Fortin, M.: "Mixed finite elements for second order elliptic problems in three variables," *Numer. Math.* (1987) **51**, 237–250.
13. Russell, T.F., and Wheeler, M.F.: "Finite element and finite difference methods for continuous flows in porous media," in *The Mathematics of Reservoir Simulation*, Frontiers in Applied Mathematics 1, Ewing, R.E., ed., Society for Industrial and Applied Mathematics, Philadelphia (1983) Chapter II, 35–106.
14. Weiser, A., and Wheeler, M.F.: "On convergence of block-centered finite-differences for elliptic problems," *SIAM J. Numerical Analysis* (1988) **25**, 351–375.
15. Arbogast, T., Wheeler, M.F., and Yotov, I.: "Mixed finite elements for elliptic problems with tensor coefficients as cell-centered finite differences," *SIAM J. Numerical Analysis* (1997) **34**, 828–852.
16. Chavent, G., and Jaffré, J.: *Mathematical models and finite elements for reservoir simulation,* Elsevier Science Publishers, New York (1986).
17. Arbogast, T., Wheeler, M.F., and Zhang, N.-Y.: "A nonlinear mixed finite element method for a degenerate parabolic equation arising in flow in porous media," *SIAM J. Numerical Analysis* (1996) **33**, 1669–1687.
18. Arbogast, T.: "Numerical subgrid upscaling of two-phase flow in porous media," in *Numerical treatment of multiphase flows in porous media*, Lecture Notes in Physics 552, Z. Chen, R. E. Ewing, and Z.-C. Shi, eds., Springer, Berlin, (2000), 35–49.
19. Arbogast, T., and Bryant, S.: "Efficient forward modeling for DNAPL site evaluation and remediation," in *Computational Methods in Water Resources XIII*, Bentley, L.R., et al., eds., Balkema, Rotterdam (2000), 161–166.
20. Peaceman, D.W.: "Interpretation of well-block pressures in numerical reservoir simulation with nonsquare grid blocks and anisotropic permeability," *SPEJ* (June 1983), 531–543.

Appendix—Derivation of the Upscaled Coarse Problem

To upscale the problem (9)–(10), we choose coarse-scale test functions. It is easier to describe the derivation if our choice of test functions is actually $w = \bar{w}_{i'}$ and $\mathbf{v} = \bar{\mathbf{v}}_{j'} + \hat{\mathbf{u}}_{j'}$, since it more readily results in a symmetric problem with respect to the velocity unknowns. Thus, using our coarse and subgrid decomposition (5) and (8) and the numerical Greens functions as in (25)–(26), we have that

$$\int a \left(\bar{P} + \hat{P}_0 + \sum_j \gamma_j \hat{P}_j \right) \bar{w}_{i'} \, dV$$

$$+ \int \nabla \cdot \left(\bar{\mathbf{u}} + \hat{\mathbf{u}}_0 + \sum_j \gamma_j \hat{\mathbf{u}}_j \right) \bar{w}_{i'} \, dV$$

$$= \int b \, \bar{w}_{i'} \, dV \, , \qquad (A\text{–}1)$$

$$\int d^{-1} \left(\bar{\mathbf{u}} + \hat{\mathbf{u}}_0 + \sum_j \gamma_j \hat{\mathbf{u}}_j \right) \cdot (\bar{\mathbf{v}}_{j'} + \hat{\mathbf{u}}_{j'}) \, dV$$

$$= \int \left(\bar{P} + \hat{P}_0 + \sum \gamma_j \hat{P}_j \right) \nabla \cdot (\bar{\mathbf{v}}_{j'} + \hat{\mathbf{u}}_{j'}) \, dV$$

$$+ \int c \cdot (\bar{\mathbf{v}}_{j'} + \hat{\mathbf{u}}_{j'}) \, dV \, . \qquad (A\text{–}2)$$

Note that in all cases

$$\int \bar{w} \, \nabla \cdot \hat{\mathbf{v}} \, dV = 0 \, , \qquad (A\text{–}3)$$

since $\hat{\mathbf{v}}$ has no flux external to the coarse block. Thus several terms cancel above. For either normalization (11) or (12),

$$\int a\,\bar{P}_j\,\bar{w}_{i'}\,dV = 0\ ,$$

so (A–1) combined with (3) and (6) gives (29).

Next we note that (21), with test function $\hat{w} = \hat{P}_j$, implies that

$$\int a\,\hat{P}_{j'}\,\hat{P}_j\,dV + \int \nabla\cdot(\bar{\mathbf{v}}_{j'} + \hat{\mathbf{u}}_{j'})\,\hat{P}_j\,dV = 0\ ,$$

so

$$\int \hat{P}_j\,\nabla\cdot(\bar{\mathbf{v}}_{j'} + \hat{\mathbf{u}}_{j'})\,dV = -\int a\,\hat{P}_j\,\hat{P}_{j'}\,dV\ . \quad (A\text{–}4)$$

Similarly, (16) with test function $\hat{\mathbf{v}} = \hat{\mathbf{u}}_{j'}$ yields

$$\int d^{-1}\hat{\mathbf{u}}_0\cdot\hat{\mathbf{u}}_{j'}\,dV$$
$$= \int \hat{P}_0\,\nabla\cdot\hat{\mathbf{u}}_{j'}\,dV + \int c\cdot\hat{\mathbf{u}}_{j'}\,dV\ . \quad (A\text{–}5)$$

Finally,

$$\int \hat{P}_0\,\nabla\cdot\bar{\mathbf{v}}_{j'}\,dV = 0 \quad\quad (A\text{–}6)$$

by normalization (11). Combining (A–2)–(A–6) results in

$$\int d^{-1}\left(\bar{\mathbf{u}} + \sum_j \gamma_j\hat{\mathbf{u}}_j\right)\cdot(\bar{\mathbf{v}}_{j'} + \hat{\mathbf{u}}_{j'})\,dV$$
$$+ \sum_j \gamma_j \int a\,\hat{P}_j\,\hat{P}_{j'}\,dV$$
$$= \int \bar{P}\,\nabla\cdot\bar{\mathbf{v}}_{j'}\,dV + \int c\cdot\bar{\mathbf{v}}_{j'}\,dV$$
$$- \int d^{-1}\hat{\mathbf{u}}_0\cdot\bar{\mathbf{v}}_{j'}\,dV\ . \quad\quad (A\text{–}7)$$

Combining now (A–7) with (3) and (6) gives (30).
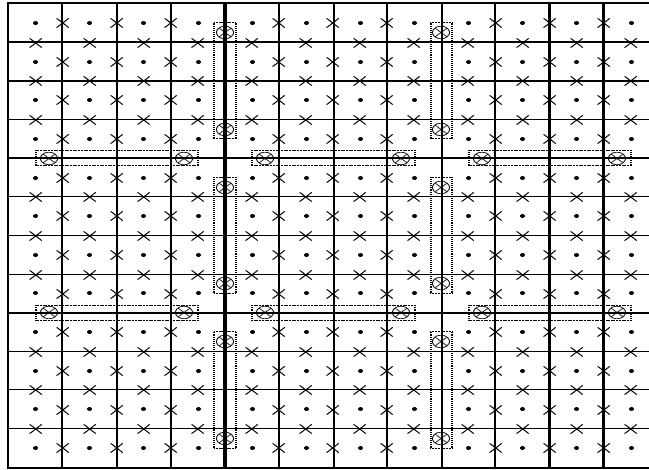
Fig. 1—A 2-D example of a 12×12 fine grid decomposed into a 3×3 coarse grid with 4×4 subgrids. The dots represent the pressure values, one per fine grid block. The crosses represent the grid block face velocity fluxes. The circled crosses apply to the coarse grid block faces, and represent linear flux variation across the face. The other crosses represent constant fluxes across the subgrid block faces internal to the coarse blocks.
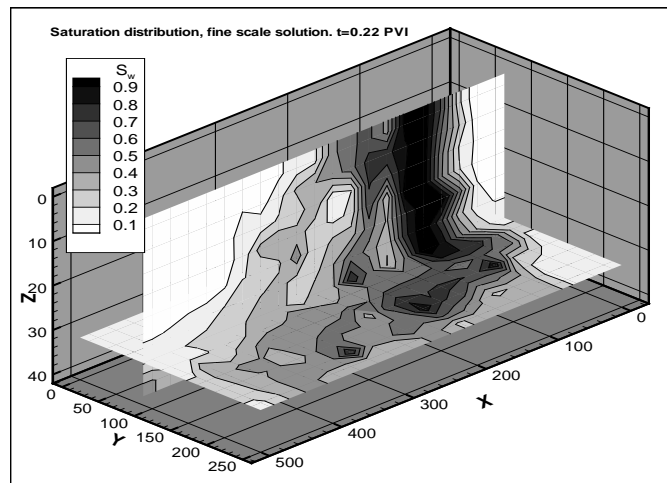

Fig. 2—Slices through a 3-D waterflood example solved on a $20 \times 10 \times 8$ grid, which we take to be the true solution. Spatial correlation in the permeability field gives rise to significant small-scale heterogeneities in the saturation distribution.
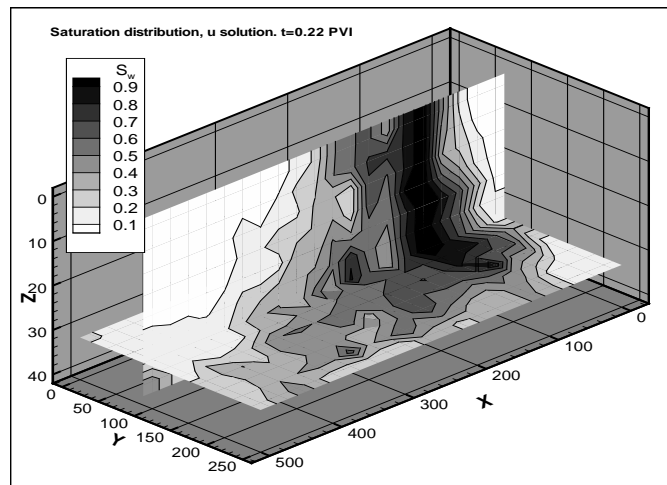
Fig. 3—Same example as in Fig. 2 solved on a 4 × 2 × 2 grid. The upscaling procedure captures much of the fine-scale behavior.
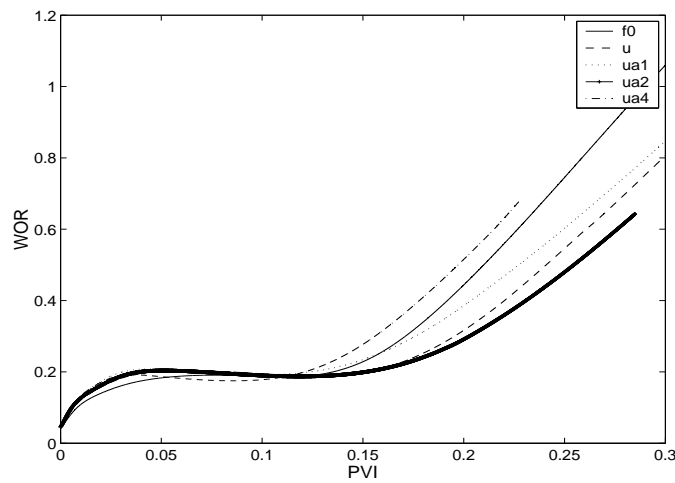
Fig. 4—Computed ratio of water production rate to oil production rate (WOR) as a function of pore volumes water injected (PVI) for a 3-D waterflood example. The fine-scale solution $f0$ is taken to be the true solution. Case u is the subgrid upscaling technique using the fine-scale permeabilities directly in coefficient d in (30). Cases $ua1$ through $ua4$ replace d with an average $\bar{d}$; the average is the arithmetic ($ua1$); harmonic in flow direction and arithmetic in the transverse direction ($ua2$); one-half power average ($ua3$); one-third power average ($ua4$).
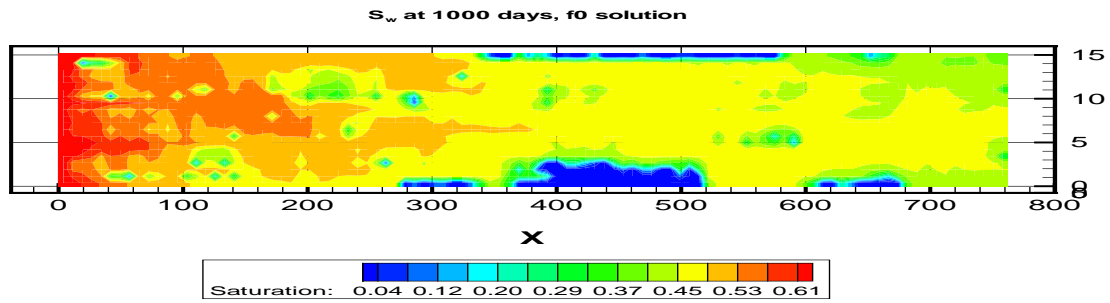
Fig. 5—Saturation distribution after 1000 days injection in a 2-D example based on the SPE comparative solution project. The solution was obtained on a 100 × 20 grid.
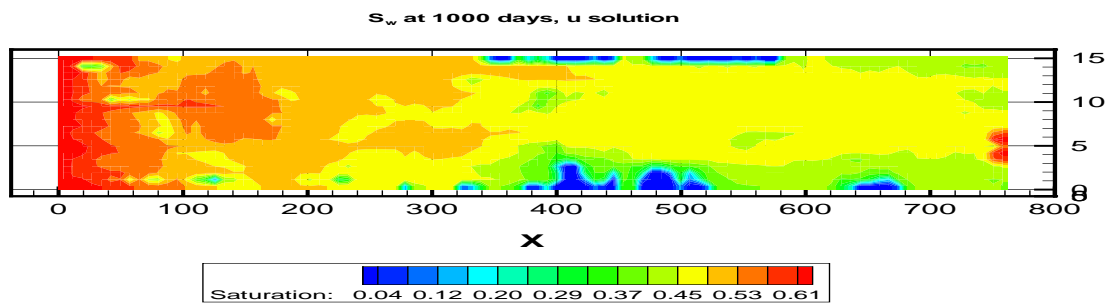

Fig. 6—Solution to the 2-D example of Fig. 5 after 1000 days injection obtained with the subgrid upscaling scheme on a 5 × 5 grid.
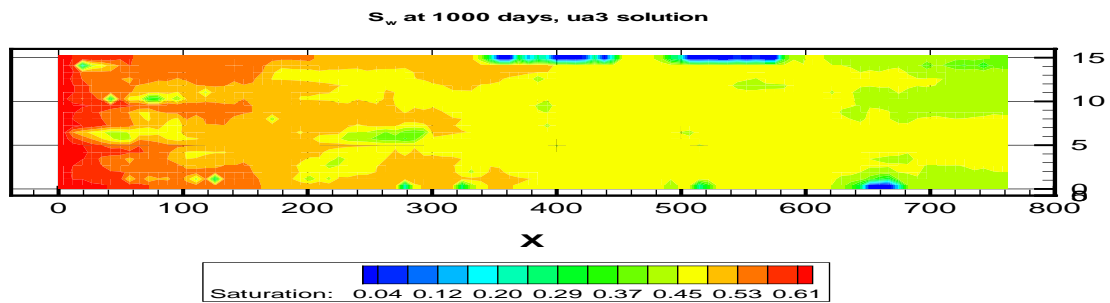

Fig. 7—Solution to the 2-D example of Fig. 5 after 1000 days injection obtained on a 5 × 5 grid, using the one-third power average permeability in the upscaling scheme.
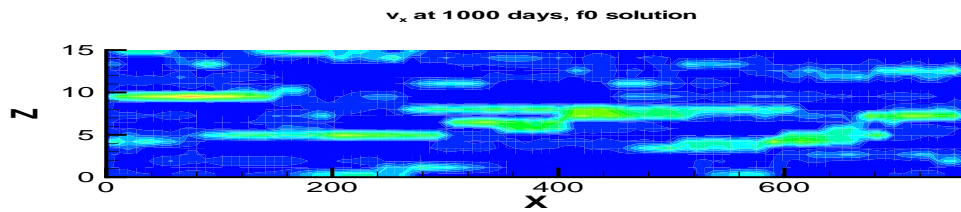
Fig. 8—Fine-scale computation of the horizontal component of the total velocity after 1000 days injection in the 2-D example of Fig. 5.
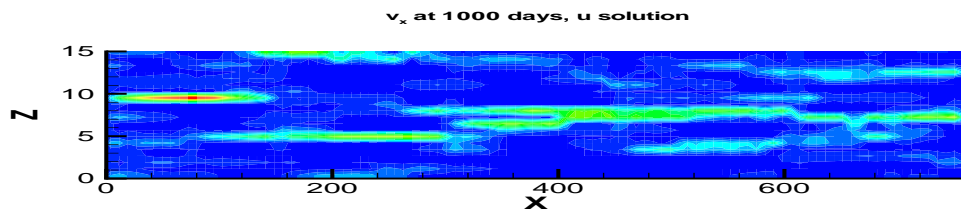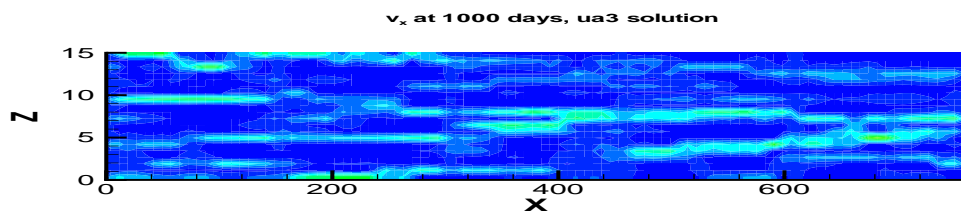

Fig. 9—Computation of the horizontal component of the total velocity after 1000 days injection in the 2-D example of Fig. 5, computed on a 5 × 5 grid with the upscaling scheme u.

Fig. 10—Computation of the horizontal component of the total velocity after 1000 days injection in the 2-D example of Fig. 5, computed on a 5 × 5 grid with the coarse-averaged permeability upscaling scheme $ua3$.